2009 IEEE International Conference on Robotics and Automation
Kobe International Conference Center
Kobe, Japan, May 12-17, 2009

Safe Robot Arm with Safe Joint Mechanism using Nonlinear Spring System for Collision Safety

Jung-Jun Park, Hwi-Su Kim, and Jae-Bok Song

Abstract—**Collision safety between humans and robots has drawn much attention since service robots are increasingly being used in human environments. A safe robot arm based on passive compliance can usually provide faster and more reliable responses for dynamic collision than an active one involving sensors and actuators. Since both positioning accuracy and collision safety of the robot arm are equally important, a robot arm should have very low stiffness when subjected to a collision force greater than the injury tolerance, but should otherwise maintain very high stiffness. To implement these requirements, a novel safe joint mechanism (SJM-II) which has much smaller size and lighter weight than the previous model, is proposed in this research. The SJM-II has the advantage of nonlinear spring which is achieved using only passive mechanical elements such as linear springs and a double-slider mechanism. Various analyses and experiments on static and dynamic collisions show that stiffness of the SJM-II is kept very high against an external torque less than the predetermined threshold torque, but abruptly drops when the input torque exceeds this threshold, thereby guaranteeing positioning accuracy and collision safety. Furthermore, a robot arm with two SJM-IIs is verified to achieve collision safety in 2D space.**

I. Introduction

In recent years, service robots have drawn a great deal of attention. Since these robots work in human environments, the safety issues related to physical human-robot interaction are increasingly important. Therefore, several types of safe robot arms have been developed for collision safety.

The safe robot arm based on passive compliance is usually composed of entirely mechanical elements such as a spring and a flexible link, which can absorb excessive collision force. Since this approach does not use any sensor or actuator, it can provide fast and reliable responses even for dynamic collision. However, a soft spring used at the joint of a robot arm leads to positioning inaccuracy due to the continuous operation of the spring even for small external forces which do not require any shock absorption. This inaccuracy is often deteriorated by undesirable oscillations caused by the elastic behavior of a spring. Although a stiff spring can provide high positioning accuracy of a robot arm, its capability of shock absorption is much lower than a soft spring, thereby giving higher probability of injury upon collision with humans. Therefore, an ideal safe manipulator would exhibit very low stiffness when subjected to a collision force greater than the injury tolerance, but would maintain very high stiffness otherwise.

To achieve this ideal feature, several variable stiffness devices based on passive compliance have been developed. A mechanical impedance adjuster with a variable spring and an electromagnetic brake was developed in [1]. A programmable, passive compliance-based shoulder mechanism using an elastic link was proposed in [2]. A variable stiffness unit with motors, two rings that consist of arc-shaped magnets and a linear guide was suggested for the safe arm of a service robot [3]. A variable stiffness actuator with the nonlinear torque transmitting system composed of a spring and a 4-bar mechanism was developed in [4]. A compliance method in the drive system which mechanically decouples the heavy actuator inertia from the link inertia was also introduced in [5]. However, in the above approaches, an extra actuator is necessary to change the joint stiffness of a robot arm, which leads to high cost, an increase in system size and weight, possible noise and malfunction of the controller.

In our previous research, this ideal feature was realized by a novel design of the safe link mechanism (SLM) and the safe joint mechanism (SJM-I) which was based on only passive compliance [6][7]. However, implementation of these safety mechanisms for the robot arm requires a compact design.

This paper presents the second version of the safe joint mechanism (SJM-II) which can be installed at the joint part of the robot arm more easily than the previous safety mechanisms. The SJM-II is mainly composed of linear springs and a double-slider mechanism. Springs are used to absorb collision force for safety, while the double-slider mechanism determines the level of external force so that the SJM-II operates only in response to a large external force. The main contribution of this proposed mechanism is the nonlinear spring capability realized using only passive mechanical elements. Without compromising positioning accuracy for collision safety, both features can be achieved simultaneously with the SJM-II. Moreover, to achieve collision safety in 2D space, the method applying several SJM-IIs to the robot arm is proposed.

The rest of the paper is organized as follows. The operational principle of the SJM-II is discussed in detail in Section II. Section III presents further explanation about the analysis of the robot arm with the SJM-II. Various experimental results for both static and dynamic collisions are provided in Section IV. Finally, Section V presents conclusions and future work.

This research was supported by Korea Science and Engineering Foundation (KOSEF) grant (R11-2007-028-01002-0) and by the Personal Robot Development Project funded by the Ministry of Knowledge Economy of Korea.

Jung-Jun Park is with the Dept. of Mechanical Eng., Korea University, Seoul, Korea (e-mail: hantiboy@korea.ac.kr)

Hwi-Su Kim is with the Dept. of Mechanical Eng., Korea University, Seoul, Korea (e-mail: fight704@korea.ac.kr)

Jae-Bok Song is a Professor of the Dept. of Mechanical Eng., Korea University, Seoul, Korea (Tel.: +82 2 3290 3363; fax: +82 2 3290 3757; e-mail: jbsong@korea.ac.kr)

II. Operational Principle of Safe Joint Mechanism-II

As mentioned in the introduction, to achieve an ideal safe manipulator, we need a nonlinear spring whose stiffness remains very high when the external force acting on the end-point of a robot arm is within the range of normal operation, but drops rapidly when the force exceeds a certain level due to collision with the object. However, no spring with this ideal feature exists. In this research, the nonlinear motion of a double-slider mechanism is exploited to achieve this nonlinear spring feature.

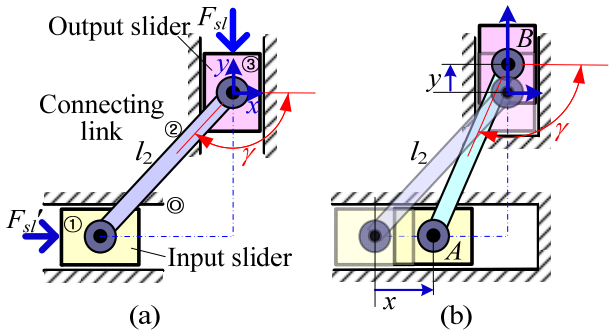

Fig. 1 (a) Double-slider mechanism, and (b) general configuration.

Figure 1 shows a general double-slider mechanism. When a slider force F_{sl} acts on the output slider (link 3) in the y-axis, an appropriate force F_{sl}' exerted on the input slider (link 1) is required for static equilibrium of this mechanism. By applying the principle of virtual work, the force ratio between F_{sl} and F_{sl}' of the double-slider mechanism can be obtained by

$$\frac{F_{sl}'}{F_{sl}} = \frac{\delta y}{\delta x} = -\cot\gamma \tag{1}$$

where δy and δx are the virtual displacements of the output slider and the input slider, respectively, and γ is the transmission angle defined as the angle between the connecting link (link 2) and the line perpendicular to the output slider movement.

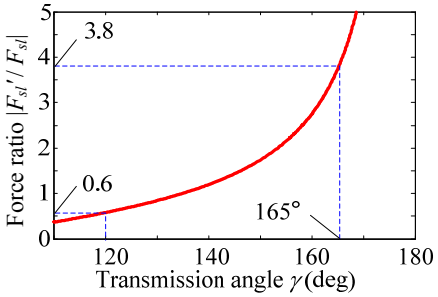

Fig. 2 Force ratio as a function of transmission angle.

As shown in Fig. 2, the force ratio varies nonlinearly depending on the transmission angle. The larger γ is, the larger the value of F_{sl}' must be to maintain equilibrium for a given F_{sl}. As γ approaches 120°, a smaller value of F_{sl}' is required for equilibrium, thereby resulting in relatively easy movement of the output slider for a given F_{sl}.

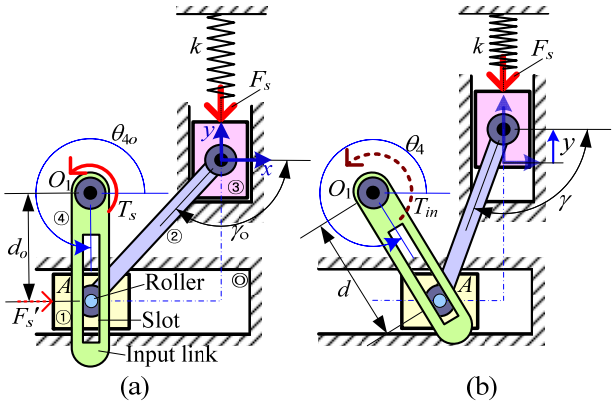

Fig. 3 Nonlinear spring system composed by a double-slider mechanism with a spring: (a) zero configuration, and (b) general configuration.

A nonlinear spring can be realized by installing a precompressed spring between the output slider and the fixed link (link 0) of the double-slider mechanism, as shown in Fig. 3. The spring force F_s can substitute for the slider force F_{sl} in Fig. 1(a) and the spring torque T_s which induces the force F_s' to the input slider can maintain static equilibrium. By applying the principle of virtual work, the relationship between T_s and F_s is obtained by

$$T_s = \frac{\delta y}{\delta \theta_4} F_s = \frac{d}{\tan\gamma \cdot \sin\theta_4} F_s \tag{2}$$

Consider a situation in which the input torque T_{in} is forced to act on the input link (link 4 in Fig. 3). Since the spring force caused by spring compression exists, the output slider does not move up until the input torque exceeds a certain threshold which generates the input torque large enough to move it up. This input torque required to initiate the movement of the output slider is defined in this paper as the *threshold torque*. Once the input torque exceeds this threshold, the spring is rapidly compressed until the output slider moves to the upmost position and the spring can no longer be compressed. From Eq. (2), the threshold torque can be described by

$$T_{th} = \frac{d_o}{\tan\gamma_o \sin\theta_{4o}} k s_o \tag{3}$$

where the subscript o represents the zero configuration, s_o is the spring compression, d_o is the displacement between points A and O_1, θ_{4o} is the angular displacement of the input link, and k is the spring constant. From Eq. (2), the equivalent stiffness seen from the input link can be obtained as a function of θ_4 as follows:

$$k_{eq} = \frac{T_s}{\theta_4 - \theta_{4o}} = \frac{d}{(\theta_4 - \theta_{4o})\tan\gamma \sin\theta_4} k(s_o + y) \tag{4}$$

where y and γ are related by $y = l_2(\sin\gamma - \sin\gamma_o)$.

For instance, when k = 5.6 kN/m, s_0 = 16 mm, l_2 = 26 mm, θ_{4o} = 270° and γ_o = 165°, the threshold torque T_{th} = 8.0 N·m. Figure 4(a) shows the relation between the spring torque T_s and the spring force F_s according to θ_4. As the angle θ_4 increases from 270° to 310°, the spring force F_s acting on the output slider increases from 90 N to 195 N because the spring is further compressed. However, T_s for equilibrium of this mechanism decreases on the contrary. For this reason the equivalent stiffness is kept very high for a small displacement of the input link, but it abruptly decreases as the angular displacement increases, as shown in Fig. 4(b). Hence, the nonlinear spring can be realized by the double-slider mechanism with a spring, which would be the main part of the SJM-II.

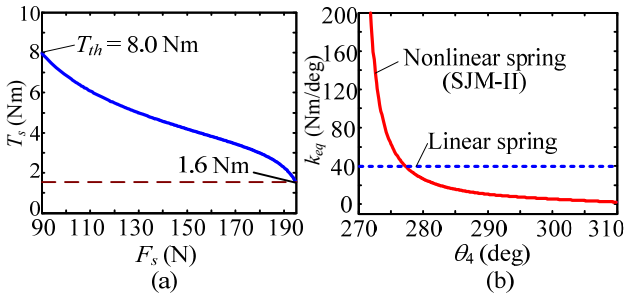

Fig. 4 (a) Spring torque versus spring force, and (b) equivalent stiffness of nonlinear spring system as a function of angle of input link.

Since the input link is a large portion of the proposed SJM-II, its mass is much larger than those of sliders and the other links in Fig. 3. Therefore, it is assumed that only the moment of inertia of link 4 is considered. In this case, the motion of the double-slider mechanism combined with a spring can be simply modeled as a 1 DOF mass-spring system, as shown in Fig. 5(a).

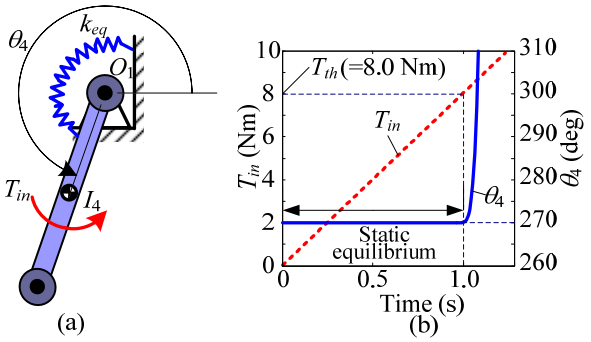

Fig. 5 Dynamic analysis of the nonlinear spring system; (a) free-body diagram, and (b) input torque and angular displacement of input link with time.

Until the input torque increases up to 8.0 N·m, which is below the threshold torque, static equilibrium of the mechanism can be maintained because the input link does not move at all, as shown in Fig. 5(b). However, as the input torque $T_{in}(t)$ increases above the threshold torque, the static equilibrium cannot be maintained and the input link starts rotating. Since the equivalent stiffness of this mechanism (k_{eq} in Fig. 4(b)) quickly decreases according to rotation of the input link, this nonlinear spring behaves as a soft spring.

III. Model of Safe Joint Mechanism-II

A. Prototype modeling

The nonlinear spring system introduced conceptually in the previous section is now realized into a new safe joint mechanism (SJM-II), which can lead to a compact and simple design of a safe robot arm. The SJM-II is composed of a double-slider mechanism, a spring and a force transmission plate, as shown in Fig. 6.

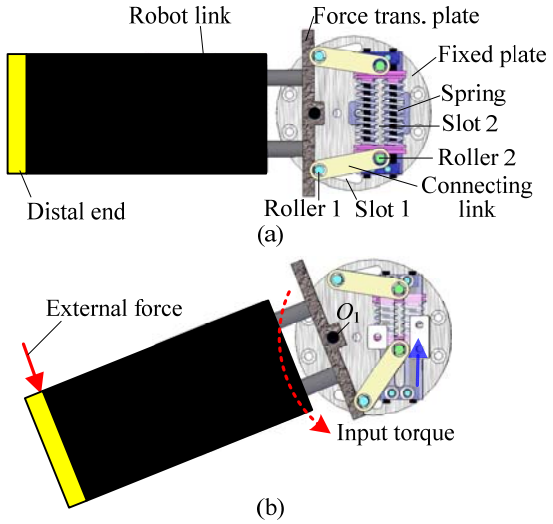

Fig. 6 Operation of SJM-II; (a) before collision, and (b) after collision.

The input slider (link 1 in Fig. 4) and the output slider (link 3 in Fig. 4) are replaced by roller 1 and roller 2 which slide along slot 1 and slot 2 of the fixed plate, respectively. The fixed plate is connected with a non-backdrivable joint actuator. The input link (link 4 in Fig. 4) is replaced by a force transmission plate. Since the force transmission plate is connected with the robot link, the external force acting on the distal end of the robot link generates the input torque which causes the force transmission plate of the SJM-II to exert the force on roller 1. Since two double-slider mechanisms which share springs are arranged symmetrically, they can absorb the external force applied in both directions.

Since the point of application of the external force is always changing, it is convenient to describe the operation of the SJM-II in terms of the input torque shown in Fig. 6(b). If the input torque exceeding the threshold torque, as shown in Fig. 6(b), then the input link is rotated around O_1. Then, roller 2 connected to the connecting link is forced to move on slot 2 in the direction of compressing the spring. As the angular displacement of the input link increases, the unbalance between the input torque and the spring torque for static equilibrium abruptly increases as introduced in section II. Therefore, the external force can be absorbed by the SJM-II. However, if the input torque is less than the threshold torque,

the distal end does not rotate at all, and the double-slider mechanism maintains static equilibrium, so the SJM-II can provide high stiffness for the joint of the robot arm.

B. Compliance analysis

Compliance analysis was conducted to verify the safety of the robot arm with one SJM-II, two SJM-IIs and without the SJM-II, respectively. The 2-DOF robot arm equipped with SJM-II was modeled as shown in Fig. 7. In this robot arm, the joint actuator composed of a motor and a speed reducer generates a torque to each joint, and the SJM-II is installed to each actuator. Note that the speed reducer has a high gear ratio as in a harmonic drive.

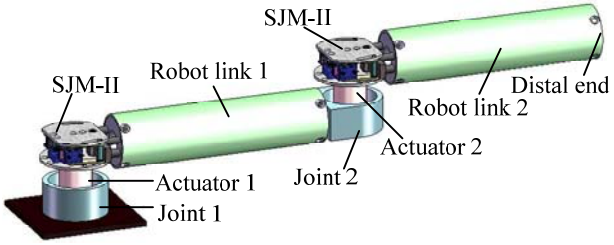

Fig. 7 2-DOF robot arm equipped with SJM.

In case of the joint without the SJM-II, the torsional stiffness of the joint is the same as that of the speed reducer. The torsional stiffness of the joint where the SJM-II is installed can be determined by the input torque acting on the robot link. If the input torque is below the threshold torque, the stiffness of the SJM-II is kept very high, so the stiffness of the joint is the same as that of the speed reducer. However, when the input torque is above the threshold torque, the stiffness of the joint becomes that of the SJM-II.

Since the stiffness of each joint is independent of each other, the stiffness matrix is given by

$$K_q = \begin{bmatrix} k_1 & 0 \\ 0 & k_2 \end{bmatrix} \tag{5}$$

The compliance matrix in the Cartesian space can be defined as:

$$K^{-1} = J K_q^{-1} J^T \tag{6}$$

where J is the Jacobian matrix. Solving the eigenvalue problem, the compliance ellipsoid can be drawn from the eigenvalues and eigenvectors. The compliance ellipsoid is useful for the safety analysis of a robot arm. The length of the major axis of the ellipsoid represents the maximum compliance, while the length of the minor axis determines the minimum compliance. Therefore, the larger the area of the ellipsoid is, the more safety is provided to the system. In this analysis, to calculate the stiffness of the SJM-II using Eq. (4), each parameter was set to the same value as in the previous section. The lengths of robot link 1 and robot link 2 are set to 350 mm and 250mm, respectively, and the stiffness of the actuators to 506 Nm/deg (=29 kNm/rad) and 77 Nm/deg (=4.4 kNm/rad).

First, the SJM-II was installed at only joint 2, and the angles of joint 1 and joint 2 were set to 0° and 45°, respectively. When the input torque due to the external force is less than the threshold torque, the stiffness of joint 2 is the same as that of the joint actuator as mentioned previously. Therefore, the area of the ellipsoid becomes very small, and consequently, high positioning accuracy of the robot arm can be achieved in normal operation without any collision, as shown in Fig. 8(a).

However, when the input torque exceeds the threshold torque, the angular displacement of the SJM-II occurs and its stiffness rapidly drops due to the operation of the SJM-II. As the angular displacement increases, the area of the compliance ellipsoid increases abruptly, as shown in Fig. 8(a). Therefore, collision safety can be improved by the use of the SJM-II.

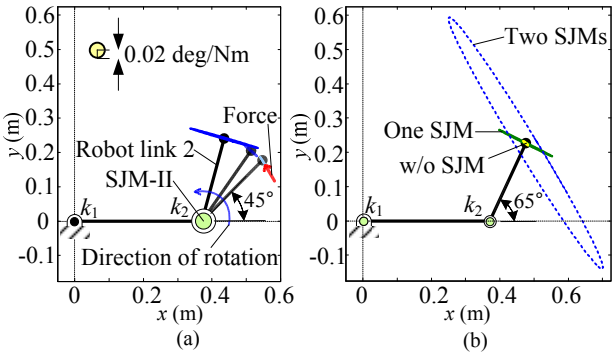

Fig. 8 Compliance ellipsoid of a robot arm equipped with SJM-II: (a) change of compliance according to external force, and (b) compliance when angle of joint 2 is 65°.

Next, to analyze safety of the robot arm with the SJM-II in 2D space, the angle of joint 2 was set to 65° and the external force was exerted on the end-point of the robot arm. As shown in Fig. 8(b), when only one SJM-II is installed at joint 2 or no SJM-II is installed, the minor axis of the ellipsoid is very short, thus maintaining very low compliance in the direction of robot link 2. However, if SJM-IIs are installed at both joints, the area of the ellipsoid becomes much larger than the cases with either no SJM-II or one SJM-II, thus providing high compliance in all directions. As a result, to ensure safety in 2D space, the SJMs should be installed at minimum two joints.

IV. Experiments for Safe Joint Mechanism-II

A. Prototype of SJM-II

The prototype shown in Fig. 9 was constructed to conduct various performance experiments related to the performance of the SJM-IIs which have the threshold torques of 12 N·m and 8.2 N·m. Most components are made of duralumin which can endure the shock exerted on the SJM-II. The sizes of SJM-IIs are ϕ65x25mm and ϕ70x35mm, and its weight is 120g and 180g, respectively. The SJM-II is more compact and

lighter than the SJM-I which is ϕ60x38mm in size, 400g in weight and 10 N·m in threshold torque. Therefore, the SJM-II can be easily installed at the joint of the robot arm.

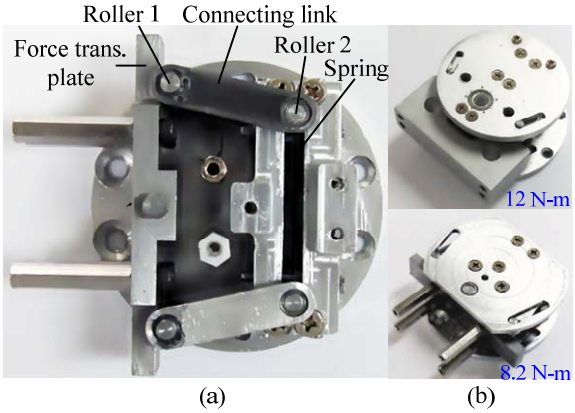

Fig. 9 Prototype of SJM-II: (a) internal view, and (b) two types of SJM-IIs.

B. *Safety criterion*

To evaluate the potential injury caused by collision, the head injury criterion (HIC) and the abbreviated injury scale (AIS) have been typically used [8]. Recently, it was claimed that those criteria are not an appropriate measure of injury severity in robotics because no robot exceeds their safety critical thresholds. This is due to much lower collision speed between a robot and a human than an automobile crash [9][10]. Therefore, the fracture force of the facial and cranial bones and the compression and viscous criterion of the chest were suggested for defining more relevant injury mechanism.

Since most service robots, unlike industrial robots, have low inertia and low speed, a lower level criterion than the fracture force limit is needed to estimate the danger of collision. Therefore, in this research, the human pain tolerance of 50N for static collision (i.e., the collision speed is below 0.6m/s) was used as the safety criterion [11].

C. *Experimental results*

Figure 10 shows an experimental setup for the 2-DOF robot arm equipped with SJM-II. The motor torque is transmitted from the speed reducer to the robot link via the SJM-II. The lengths of robot link 1 and robot link 2 are 37cm and 25cm, respectively. Collision force between the end-point and the wall is measured by a force/torque sensor installed at the fixed wall.

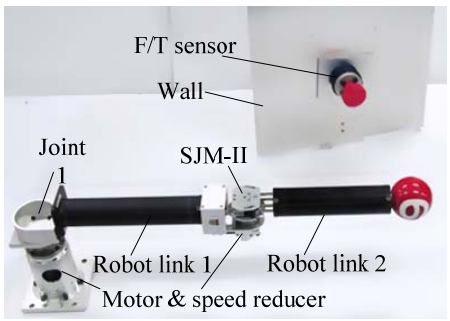

Fig. 10 Experimental setup for robot arm with SJM-II.

First, to evaluate the performance of the SJM-II, experiments were conducted for the robotic arms with and without SJM-II (T_{th} = 8.2 N·m) installed at only joint 2. In the experiment for static collision, the angle of joint 2 was set to 0°, the end-point of the robot arm was initially placed to barely touch a fixed wall, and the torque of joint 1 provided by the motor was slowly increased.

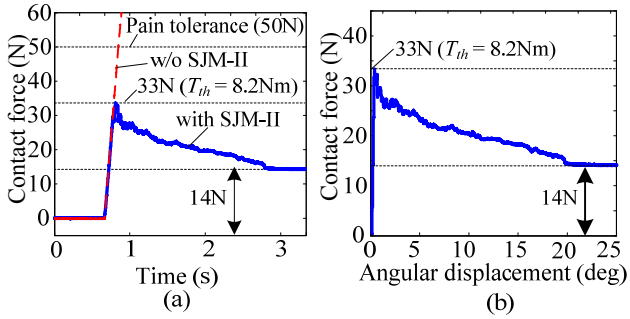

Fig. 11 Experimental results for static collision for robot arm: (a) collision force versus time with and without SJM-II, and (b) collision force versus angular displacement of SJM-II.

As shown in Fig. 11(a), the robot arm without the SJM delivered a contact force that increased up to 60 N to the wall due to high stiffness of the speed reducer. However, a contact force of only up to 33 N was transmitted to the wall for the robot arm with SJM-II, although the motor continually rotated after collision, the contact force decreased to 14 N. In other words, the contact force above pain tolerance does not occur because the excessive force is absorbed by the SJM-II.

In Fig. 11(b), virtually no displacement of the robot arm occurs when the external torque due to the contact force is below the threshold force of 33 N. Therefore, the robot arm with SJM-II can accurately handle a payload up to approximately 3 kg as though it had a speed reducer with a high gear ratio. As the input torque increases above the threshold torque, the stiffness of joint 2 due to SJM-II quickly diminishes, thus absorbing the collision force so that the transmitted force is below the pain tolerance.

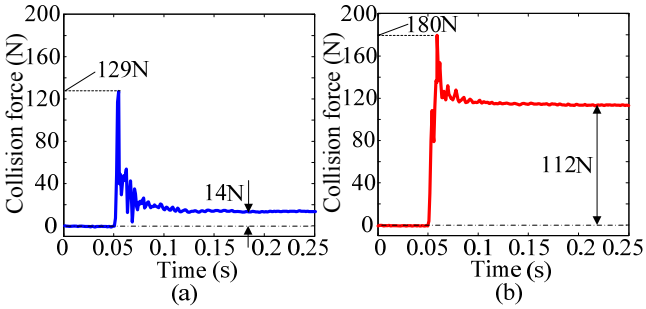

Fig. 12 Experimental results on dynamic collision; (a) with SJM-II, and (b) without SJM-II.

For dynamic collision, when joint 1 rotated at an angular velocity of 90 °/s, which corresponds to the end-point velocity of 1 m/s, the end-point of the robot arm was forced to collide with a fixed wall. At the instant the robot arm equipped with SJM-II collided with the wall, the peak value of the collision force reached 129 N which is less than that without SJM-II,

but immediately after collision, the collision force delivered to the wall dropped to 14 N due to the operation of the SJM-II. In case of the robot arm without SJM-II, the collision force after collision was more than the human pain tolerance of 50 N. Therefore, the robot arm with the SJM-II provides much higher safety for human-robot contact than that without the SJM-II.

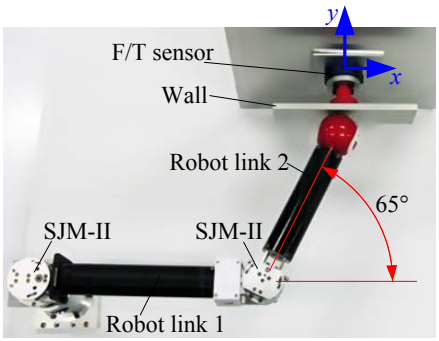

Fig. 13 Experimental conditions for collision safety of robot arm in 2-D space.

Next, to verify the effect of the robot arm with SJM-II in 2D space, some experiments were conducted. The angle of joint 2 was set to 65°, and the fixed wall where the F/T sensor was installed was aligned in accordance with the *x*-*y* axis, as shown in Fig. 13. For static collision of the robot arm without SJM-II, the contact force in both *x* and *y* directions increased up to the pain tolerance, as shown in Fig. 14(a). When the SJM-II was installed at only joint 2 of the robot arm, the contact force in the *y* direction increased up to the pain tolerance. However, when the SJM-II was installed to each joint, the contact force was transmitted only up to 32 N in the *y*-direction and 8 N in *x*-direction, which were below the pain tolerance. Therefore, the safe human-robot contact can be achieved even in 2D space using two or more SJM-IIs at each joint.

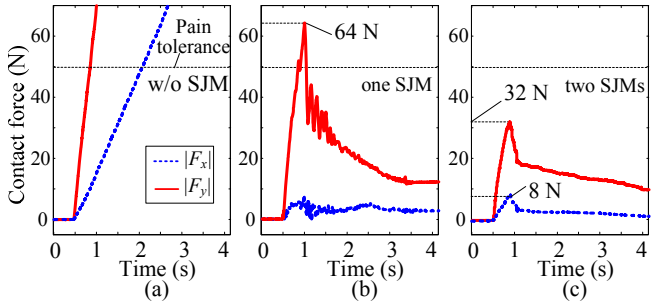

Fig. 14 Experimental results on static collision; (a) without SJM, (b) with one SJM-II, and (c) with two SJM-IIs.

V. Conclusions

In this research, the second version of a safe joint mechanism (SJM-II) was proposed for collision safety. The robot arm equipped with the SJM-II can simultaneously provide both positioning accuracy and collision safety. From the analysis and experiments, the following conclusions are drawn:

1) High stiffness of the robot arm can be maintained for the low input torque that is lower than the threshold torque, which can achieve positioning accuracy in normal operation.

2) Stiffness of the robot arm abruptly drops if the input torque to the SJM-II exceeds the pre-determined threshold torque. Therefore, collision safety can be achieved even for a high-speed dynamic collision.

3) Since the SJM-II permits rotation of 1 DOF, the collision safety in 2D space can be achieved by simply applying two SJM-IIs to the robot arm.

Currently, a safe robot arm with safe joint mechanisms is under development to achieve collision safety in 3D space.

References

[1] T. Morita and S. Sugano, "Development and evaluation of seven DOF mia arm," *Proc. of the IEEE International Conference on Robotics and Automation*, pp. 462-467, 1997.

[2] M. Okada, Y. Nakamura and S. Ban, "Design of programmable passive compliance shoulder mechanism," *Proc. of the IEEE International Conference on Robotics and Automation*, pp.348-353, 2001.

[3] J. Choi, S. Park, W. Lee, and S. Kang, "Design of a Robot Joint with Variable Stiffness," *Proc. of the IEEE International Conference on Robotics and Automation*, pp. 1760-1765, 2008.

[4] R. Schiavi, G. Grioli, S. Sen and A. Bicchi, "VSA-II: a Novel Prototype of Variable Stiffness Actuator for Safe and Performing Robots Interacting with Humans," *Proc. of the IEEE International Conference on Robotics and Automation*, pp. 2171-2176, 2008.

[5] M. Zinn, O. Khatib, B. Roth and J. K. Salisbury, "A new actuation approach for human-friendly robot design," *International Journal of Robotics Research*, vol. 23, no. 4/5, pp. 379-398, 2005.

[6] J.-J. Park, B.-S. Kim, J.-B. Song and H.-S. Kim, "Safe Link Mechanism based on Nonlinear Stiffness for Collision Safety," *Mech. Mach. Theory* (2007), doi:10.1016/j.mechmachtheory. 2007.10.004.

[7] J.-J. Park, Y.-J. Lee, J.-B. Song and H.-S. Kim, "Safe Joint Mechanism based on Nonlinear Stiffness for Safe Human-Robot Collision," *Proc. of the IEEE International Conference on Robotics and Automation*, pp. 2177-2182, 2008.

[8] J. Versace, "A review of the severity index," *Proc. of the 15th Stapp Car Crash Conference*, pp.771–796, 1971.

[9] S. Haddadin, A. Albu-Schaffer, and G. Hirzinger, "The Role of the Robot Mass and Velocity in Physical Human-Robot Interaction – Part I: Non-constrained Blunt Impacts," *Proc. of the IEEE International Conference on Robotics and Automation*, pp. 1331-1338, 2008.

[10] S. Haddadin, A. Albu-Schaffer, and G. Hirzinger, "The Role of the Robot Mass and Velocity in Physical Human-Robot Interaction – Part II: Constrained Blunt Impacts," *Proc. of the IEEE International Conference on Robotics and Automation*, pp. 1339-1345, 2008.

[11] Y. Yamada, Y. Hirasawa, S.Y. Huang and Y. Umetani, "Fail-safe human/robot contact in the safety space," *IEEE International Workshop on Robot and Human Communication*, pp. 59-64, 1996.